Proceedings of GPPS Forum 18
Global Power and Propulsion Society
Zurich, 10th-12th January 2018
www.gpps.global

GPPS-2018-0047

AERODYNAMIC INVESTIGATION OF AN EMBEDDED UHBR-ENGINE CONCEPT

Constance Heykena
Institute of Jet Propulsion and Turbomachinery
c.heykena@ifas.tu-braunschweig.de
Braunschweig, Germany

Jens Friedrichs
Institute of Jet Propulsion and Turbomachinery
j.friedrichs@ifas.tu-braunschweig.de
Braunschweig, Germany

ABSTRACT

To cope with the changing demands in air transport the Collaborative Research Centre (CRC) 880 emphasis future development of technologies for the application on a cruise efficient transport aircraft. The future aviation challenges like the reduction in fuel consumption and noise emission shall be met by a transport aircraft design with short take-off and landing capabilities. Part of this concept is to mount the aircraft propulsion system on the wing aft of its trailing edge. Nacelles mounted over-the-wing cannot only offer benefits in noise reduction due to shield effects by the wing but also have the potential to accommodate aircraft engines with growing engine diameters without any ground clearance restrictions. Moreover, a possible synergy between the wing flowfield and nacelle inlet might lead to a short nacelle design which is crucial for increasing bypass ratios of turbofan engines. Within the presented numerical study, a preliminary design of an embedded Ultra-High-Bypass-Ratio-engine (UHBR) was investigated to evaluate the corresponding flow phenomena for an on-wing-nacelle (OWN) at high speed conditions. The axial position of the engine will be varied at constant lift. The results show that the aircraft performance improves in terms of angle of attack and drag by shifting the nacelle axially downstream.

INTRODUCTION

For the future in aviation ACARE [European Commission, 2011] demands a drastic reduction in fuel and noise reduction by 2050. In response to this claim the CRC 880 objective is to investigate and assess new technologies for a STOL concept aircraft (Radespiel et al., 2017; Delfs et al., 2017). A key feature of this vehicle is the active high lift system which ensures a runway length of less than 900 meters during take-off and landing. This prerequisite is supposed to answer the growing demand on point-to-point connections and make small airports close to residential areas operable.

For the presented concept one part of the solution to combat the challenges of fuel and noise reduction is to increase the bypass ratio (BPR) of the aircraft engine and change the common engine position to an over-the-wing mounted nacelle. This installation position of the propulsor offers a variety of advantages such as noise reduction due to shielding effects, a reduction of landing gear length and thus weight. In addition to this, on-wing-nacelles can accommodate engines with growing sizes which is a result of the increase in BPR. These benefits used to be offset by a poor performance in aerodynamic behaviour. However, recent studies have shown that rear mounted OWN installations can also hold the potential for increasing BPR to improve the performance in aircraft aerodynamics (Hooker et al., 2013). Fujino and Kawamura, 2003, found the potential of wave drag reduction for a business jet application by locating the nacelle on the wing. They proposed to put the nacelle front face close to the shock position of the clean wing to decrease drag due to aerodynamic interference.

Figure 1 Overview of Configuration

Presently, pylons are commonly used for mounting engines on most transport aircraft. Within the presented study, a closer coupling between the aircraft and engine is chosen by embedding the nacelle into the wing. Beside the already mentioned benefits of OWN this approach is supposed to counter the growing nacelle dimensions. It is commonly known that the aircraft engine efficiency can be improved by increasing the BPR. A higher BPR causes the fan diameter to increase as well. From the nacelle point of view a longer inlet length is then required as well, because this parameter has a strong influence on the inlet flow conditions at the fan. The presented concept aims for a synergy of wing and nacelle interaction to shorten the inlet length due to the positive influence of the wing. An overview of the investigated concept is depicted in Figure 1.

In the following, a numerical preliminary sensitivity analysis of an embedded UHBR-engine on a transport aircraft at high flight Mach numbers at cruise altitude will be presented. Aircraft performance is evaluated with respect to the wing's upper surface pressure distribution as well as the nacelle cowling pressure distribution at the 12 o'clock position. The results of this preliminary integration approach provide a basis to derive a design methodology for the embedded nacelle proposed within this concept.

METHODOLOGY

To perform and evaluate numerical engine integration studies, an aircraft model and an engine model are required as a reference. This section continues with a general description of the aircraft and engine integration approach. Further, the numerical setup will be presented.

Baseline aircraft and nacelle configuration

The transport aircraft concept investigated in this study is sized for a short distance mission with 100 PAX and 45t max. payload. It is a low wing configuration featuring a span of 28.745m and reference area of 99 m^2. Since the cruise flight speed is Ma = 0.78 the wing features a swept of 26 deg. The two UHBR engines are installed at 31 % of the wing's span. This position also accommodates the pylon integrated landing gear. A detailed description of the transport aircraft can also be found in Heinze and Weiss, 2015. At this phase of the project the vertical and horizontal stabilizers are omitted for the numerical studies as shown in Figure 1.

The thrust requirement for the design of the engine cycle is derived by the aircraft mission profile. The engine's thermodynamic cycle determines the relevant dimensions at the fan inlet and separated nozzle configuration and the corresponding boundary conditions for the numerical simulation. The engine design data is required as an input for the surface model generation of the isolated generic UHBR nacelle.

The clean Wing-Body configuration (WB) and isolated nacelle will be used as a baseline for the assessment of the following integration studies.

Propulsion integration approach

For a preliminary evaluation of a highly integrated UHBR nacelle in an over-the-wing position a parameter study was conducted. The spanwise position of the integrated engine was kept constant at $\eta = 0.31$ of the wing's span, which is prescribed by the aircraft design. The chordwise position of the propulsor was varied. The reference of the nacelle in axial position is the fan face of the engine, where the flow enters the inner part of the propulsion. The placement study was done with the nacelle being varied from 84 % to 100 % of the local chord length at this wing section. For all positions the fan was directly above the wing's upper surface, which determined the vertical position of the engine. Since the nacelle is placed in the sensitive transonic regime of the upper wing's flowfield the step size was chosen to be 2% to catch possible occurring phenomena. Figure 2 illustrates the cross section of the investigated configuration at $\eta = 0.31$. The profile of the wing, which is coloured in white, remains unchanged for this study. This is to investigate the fundamental changes in the upper surfaces flowfield due to the installation effect of the OWN. Hence, the lower part of the nacelle is trimmed and a junction between wing and nacelle designed. The grey area in Figure 2 shows a cut through the engine model being used and the integrated landing gear. The position of the propulsion system is with the fan face being at 100% of the local chord length of the wing, declared as $x_{Fan} = 1$.

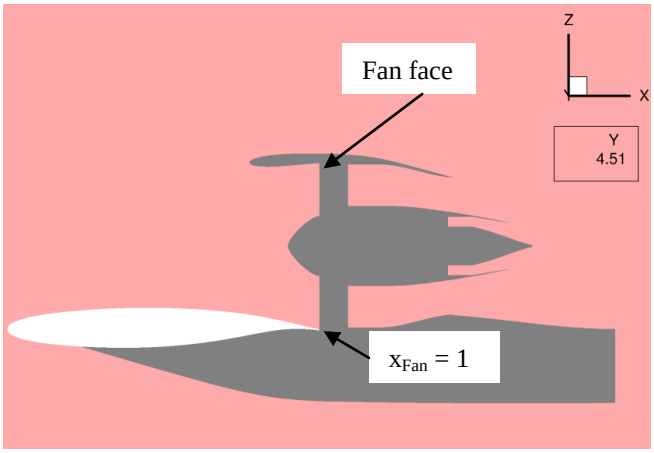

Figure 2 Cross section through embedded propulsor at η = 0.31

Different junctions between wing and nacelle were tested all of them leading to separations at both sides of the nacelle. This leads to the assumption that the separation can only be eliminated by a shape optimization of the nacelle profile on both sides due to the strong impact of the wing's flowfield. Figure 3 illustrates the chosen junction between wing and nacelle. This means on the other hand that the presented parameter study was conducted even though separations occurred on the outer part of the nacelle. The focus of this study is to assess the impact of the highly integrated nacelle on the flowfield of the wing and upper nacelle for deriving design parameters for a future embedded nacelle design which is claimed to eliminate flow separation.

The objective of this study is to find an appropriate starting point with respect to the engine position as a basis for future optimization in shape design of the nacelle.

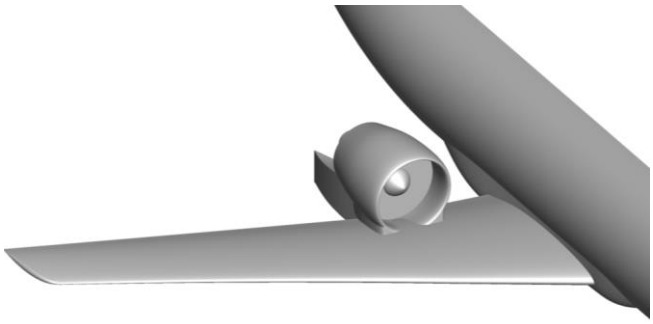

Figure 3 View on embedded nacelle

Numerical Approach

All surface models were created with the commercial CAD software CATIA V5R21. To safe computational resources the clean WB as well as the integration studies were carried out on a half model of the Wing-Body-Engine (WBE) configuration while the isolated nacelle was done on a full model. The computational grids are all hybrid and done by using the commercial grid generator centaur (CentaurSoft, 2017) since it can be easily adapted to geometrical changes. Mesh sizes were around 5 million nodes for the isolated nacelle, around 9 million nodes for the WB and around 19 million nodes for the WBE. The boundary layer was discretised with 37 prism layers with the first cell sizes chosen to match a $y^+ = 1$.

The CFD simulations were conducted with the 3D steady Reynolds Averaged Navier Stokes (RANS) solver DLR-TAU code (DLR, 2014). For the spacial discretization an upwind schema was chosen while for the turbulence modelling Menter Shear Stress Transportation model (Menter, 1994) was used. Viscous walls were considered to be fully turbulent without transition since the Reynolds number for the tested case was about 21×10^6.

Boundary condition

All computations were conducted with a farfield boundary condition. The cruise flight altitude is 11,277 m and the atmospheric conditions were set accordingly. As already mentioned the design speed of flight is Ma = 0.78. At this operating point each UHBR-engine demands a massflow of $\dot{m}$ = 202.92kg/s at the fan inlet which was used as fan face boundary condition. The jet streams of the separated nozzle at the rear of the nacelle were realized by prescribing both, a temperature and pressure ratio for each nozzle to meet the thrust requirement of F = 16 kN at this operating point.

RESULTS AND DISCUSSION

In this section the results of the simulation of the clean WB and nacelle are shown first in terms of isobars and pressure distribution. Afterwards, the nacelle will be integrated into the rear part of the wing as shown in Figure 2 and Figure 3 and the axial position will be varied. The WBE will be compared to the clean WB and isolated nacelle for Ma = 0.78. At last, a variation of flight Ma number will be presented.

Results of clean WB and isolated nacelle

Figure 4 depicts the isobars for the WB configuration at the design cruise speeds of the presented aircraft concept at Ma = 0.78. A shock at about 75 % of the wing chord extends from the wing root to tip. To reach the target lift coefficient of $C_L = 0.46$ an angle of attack $\alpha = 1.9$deg is required.

In accordance to the WB Figure 5 shows the isobars on top of the isolated nacelle. Since the engine will be embedded with no incidence or toe angle the boundary condition in terms of angle of attack for this simulation were set to $\alpha = 0$deg. Both simulation results serve as a reference for the following integration study.

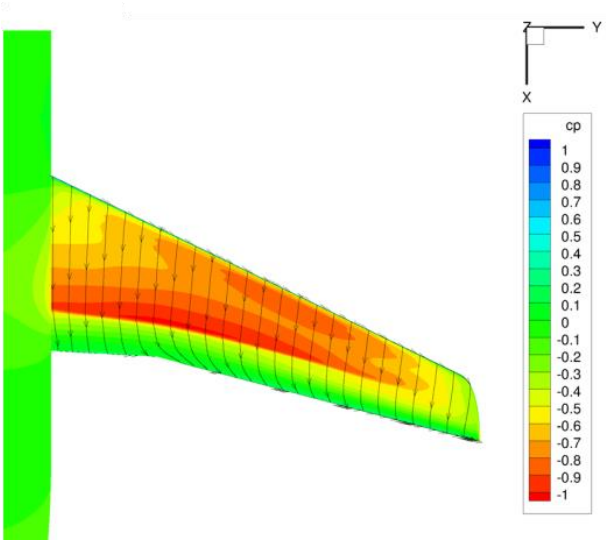

Figure 4 Pressure isobars on upper wing surface for Ma = 0.78

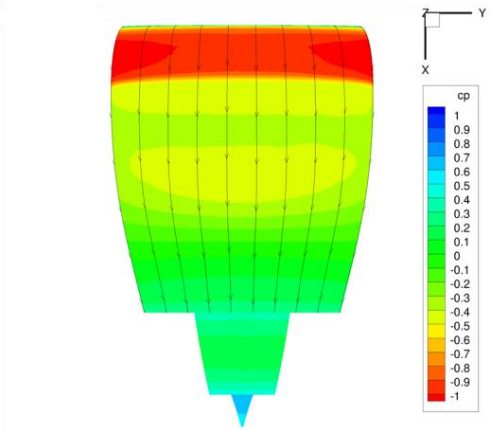

Figure 5 Isobars of isolated nacelle (view on the 12 o'clock section)

Results of integration study

The parameter study was carried out for an x-position x_{Fan} of the engine varying from 0.84 to 1 of the local chord for high-speed conditions. The simulation target was to reach a target lift coefficient of $C_L = 0.46$, which is required by the aircraft design.

Chordwise variation results for Ma = 0.78

Installing the engine on the upper wing surface leads for a constant lift to an increase in angle of attack. For the design cruise point the angle of attack rises to 4.5deg for x_{Fan} = 0.84 and to 3.9deg for x_{Fan} = 1. In between these two engine positions a nearly linear relation establishes, which is shown in Figure 11. This is why in the following only the extreme positions at x_{Fan} = 0.84 and x_{Fan} = 1 will be further discussed.

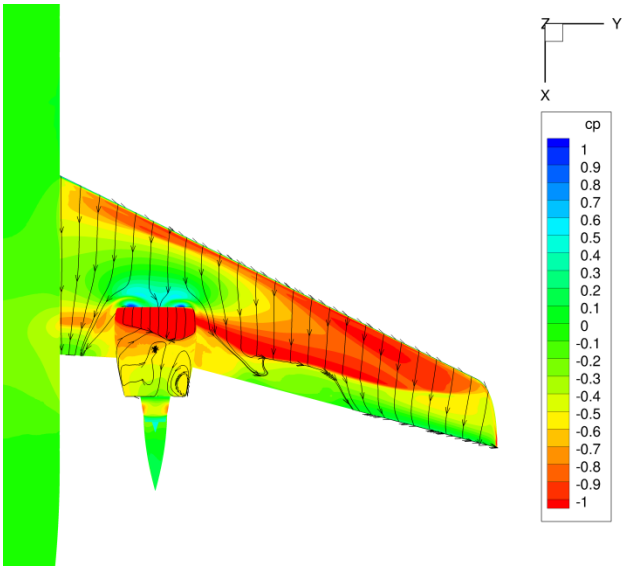

Figure 6 Isobars and skin friction lines of WBE with engine at x_{Fan} = 0.84

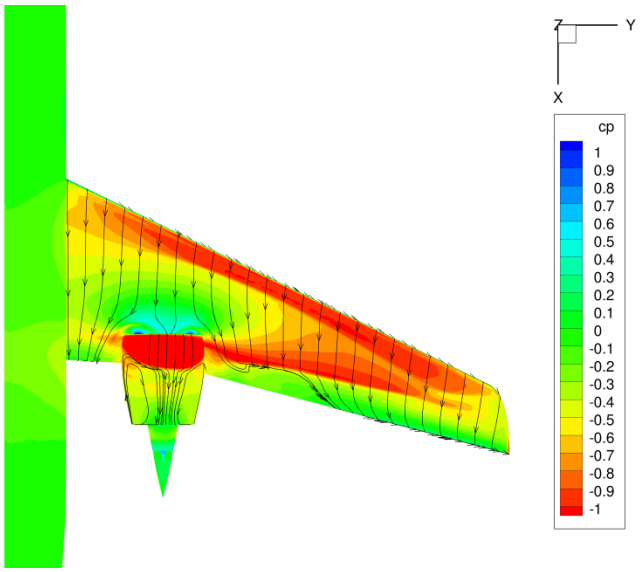

Figure 7 Isobars and skin friction lines of WBE with engine at x_{Fan} = 1

The WBE configuration with x_{Fan} = 0.84 in Figure 6 illustrates the impact of the engine on the wing in terms of isobars and skin friction lines. With respect to the WB shown in Figure 4 the approaching flow is decelerated by the OWN leading to a mitigation of the shock in the area where the engine is installed. For the mid part of the wing a shock induced separation indicated by the skin friction lines on the wing surface occurs while on the outer wing part a double shock can be found. The shock on the nacelle surfaces moves down in flow direction compared to the isolated configuration shown in Figure 5. The skin friction lines reveal the areas of flow separation. After the shock the flow on the nacelle is detached completely.

Shifting the nacelle further downstream alleviates the flow separation on wing and nacelle, resp., which can be seen in Figure 7. In addition, the interaction of nacelle and fuselage, is not as strong as shown in Figure 6 at x_{Fan} = 0.84. The flow between nacelle and fuselage is not as strongly accelerated as for x_{Fan} = 1, which is also depicted in the c_p distribution shown in Figure 8. As a result, the shock induced separation on the nacelle becomes weaker. Figure 7 also shows a smaller area of separation in the mid part on the wing. Hence, shifting the installation position of the engine to the rear of the wing has a positive effect on both components. This might also be the reason for the decreasing drag of the configuration, which is in accordance with the angle of attack shown in Figure 12.

The local c_p distribution at different sections of the wing at Ma = 0.78 are depicted in Figure 8 for x_{Fan} = 1 (red curves) and x_{Fan} = 0.84 (green curves). Both WBE configurations are compared to the clean wing of the WB (black curves).

The section at η = 0.31 shows the decelerating effect of the installed engine on the upper wing surface as well as the impact of adding the landing gear on the lower wing surface. For the WB there is a shock located at 0.75 of the local wing chord. For the WBE configurations the influence of the OWN causes the shock to move upstream to 0.2 of the local wing chord for x_{Fan} = 1 and 0.1 for x_{Fan} = 0.84 with the shock being more intense for the latter. The lift for this section drops in regard to the WB for both configurations being more significant for the position further upstream.

By comparing the c_p distributions at η = 0.21 the deceleration effect of the OWN becomes obvious again. At this part of the wing, the shock, which is present for the WB configuration, disappears when installing the engine. Instead, the flow slows down until it passes the front face of the nacelle and is then accelerated again. A similar behaviour shows the distribution at η = 0.5, the only difference at this wing section is a first shock which is located at 0.15 of the local chord for x_{Fan} = 0.84 and 0.2 for x_{Fan} = 1. The flow is then again accelerated when passing the nacelle which causes another shock leading to a flow separation. Due to the installation effect of the nacelle, the inner part of the wing creates less lift with respect to the reference WB configuration.

Looking at the outer sections η = 0.7 and η = 0.9 the c_p curves demonstrate that in relation to the WB these sections are aerodynamically higher loaded to compensate for the loss in lift caused by the engine installation at the inner wing part. When comparing Figure 7 and Figure 6 the isobar patterns on the wing look in principle similar. However, the further upstream the engine is placed, the stronger the decelerating effect in front of the engine affects the lift creation, which can also be seen in the c_p curves. This is one explanation for the increasing angle of attack to reach the required target C_L when shifting the OWN axially upstream.

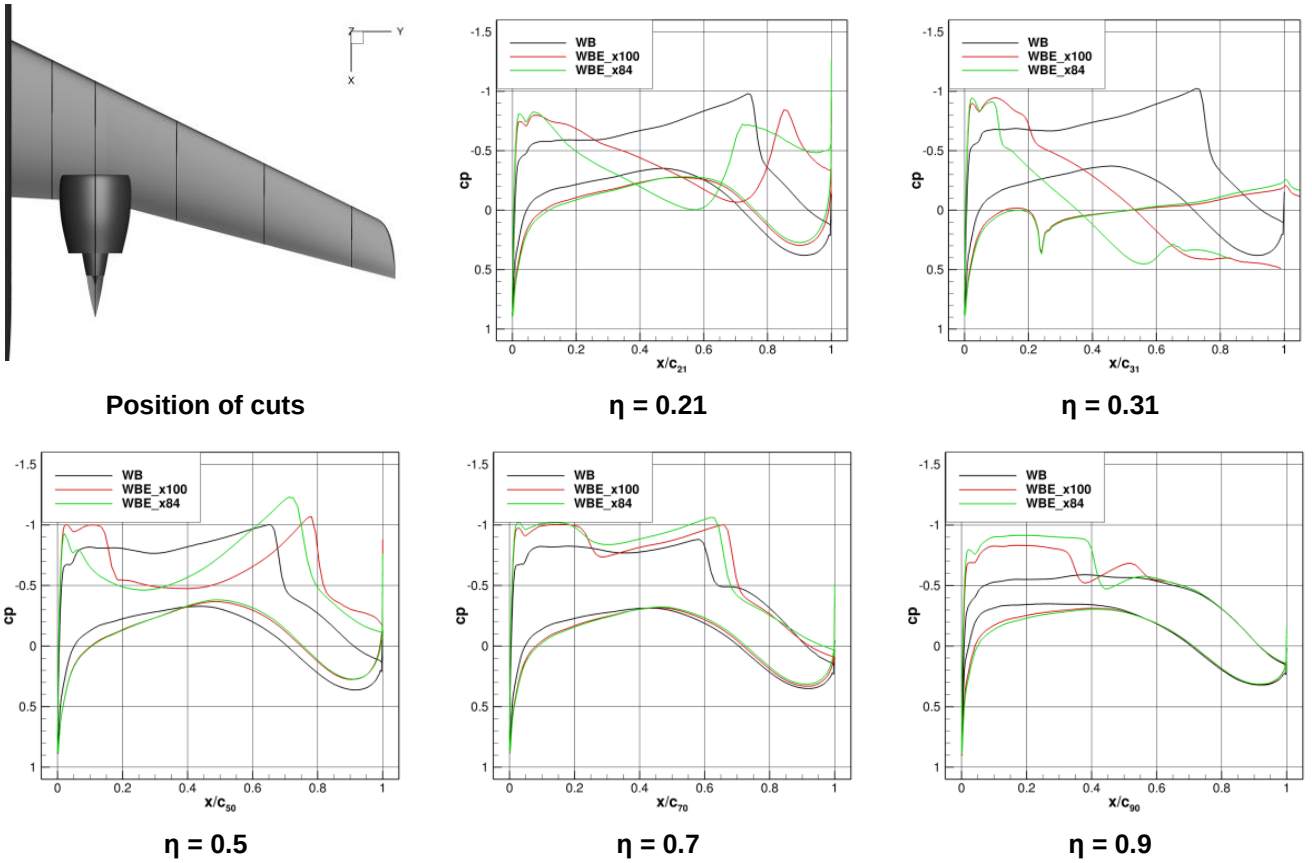

Figure 8 Pressure coefficient of WBE and WB at different wing sections

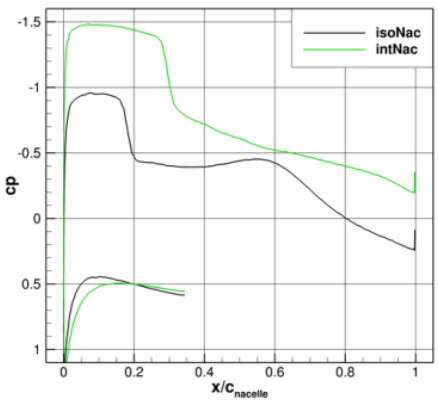

Figure 9 c_p distribution of isolated and integrated nacelle at 12o'clock for x_{Fan} = 0.84

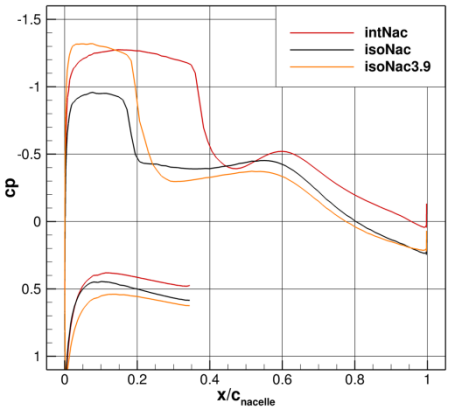

Figure 10 c_p distribution of isolated and integrated nacelle at 12o'clock for x_{Fan} = 1

The results of the isolated (black) and integrated nacelle (color) are compared in Figure 9 and Figure 10. The section at η = 0.31 is evaluated for the upper part of the nacelle, which is from a circumferential point of view at 12 o'clock position of the nacelle. The resulting c_p distribution illustrates that this part of the integrated OWN is higher loaded with respect to the isolated nacelle. The shock occurring on both, the isolated and integrated nacelle moves down axially for x_{Fan} = 0.84 by $\Delta c_{nacelle}$ = 0.125 in Figure 9 and $\Delta c_{nacelle}$ = 0.2 for x_{Fan} = 1 in Figure 10, red curve, resp.

Due to the impact of the wing the position of the shock changes for the integrated nacelle and leads as a consequence to a higher proportion of lift generated by the nacelle.

Since each investigated WBE configuration operates at a different angle of attack an additional isolated nacelle simulation was conducted for the best performing configuration of the evaluated parameter space at x_{Fan} = 1. The resulting angle of attack equals 3.9deg for the WBE simulation to reach target lift. The resulting c_p distribution of the isolated nacelle for this angle of attack is depicted in Figure 10's, orange curve. When comparing the results for

the isolated and embedded nacelle it can be found that the position of the shock established further downstream for the embedded configuration.

Mach number variation

To investigate the influence of the speed of flight a variation of Ma number was carried out. Beside the design Ma number four additional ones were to be simulated keeping the target C_L and engine boundary conditions constant. The resulting angle of attack α for each speed of flight and x-position is depicted in Figure 11. The chart establishes that all speed of flight have the same trend, which was already discussed for Ma = 0.78. The further aft the nacelle is placed the lower the resulting angle of attack. This means, that for the analysed parameter space $x_{Fan} = 1$ is the best performing position in terms of angle of attack for all Mach numbers.

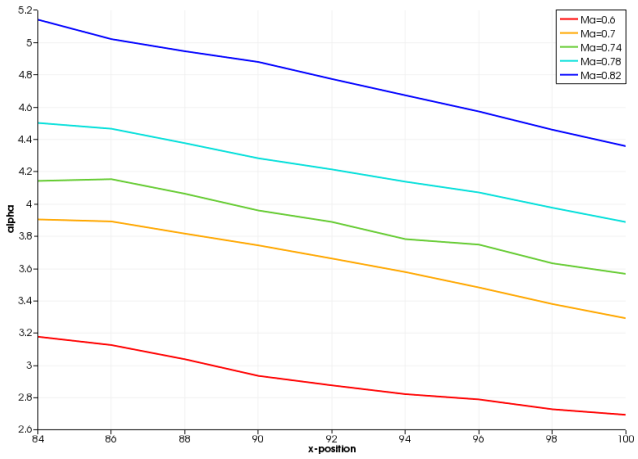

Figure 11 Angle of attack over engine position for different Ma numbers

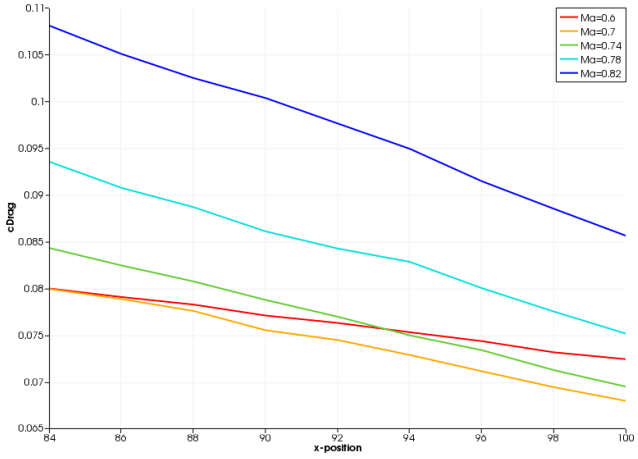

Figure 12 Drag coefficient C_D over engine position for different Ma numbers

Having a look on the resulting drag of the WBE a similar trend can be observed. Figure 12 shows the resulting drag coefficient C_D graphs over the engine positions for each investigated Mach number. By shifting the engine down in axial direction, the resulting C_D decreases. This again suggests that an engine position further down the wing is favourable.

The absolute value of the graphs' slopes rises for increasing Ma numbers. The slope of the resulting curve for Ma = 0.6 shows, however, that the drag reduction by placing the engine further down the wing is not as intense compared to the other higher speed of flights. This leads to the assumption that the potential of a rear mounted OWN in terms of drag reduction might only be applicable for higher speed of flights when transonic flow areas are present.

Due to the separation areas occurring for the integrated OWN the total amount of drag almost triples with respect to the clean aircraft for $x_{Fan} = 1$ at the design speed of flight, which is not feasible. This underlines the need for an improved design of the nacelle shape especially in the area of the junction to the wing.

CONCLUSIONS

The results of a numerical study for an aircraft concept with an over-the-wing embedded propulsion system were investigated for high speed conditions. For the tested parameter space at the rear part of the wing the further down the wing the engine was placed the better the performance of the configuration in terms of angle of attack and drag became. The potential of this configuration design lies in the nacelle having a share in the generation of lift. In this study, an optimized wing for an under-the-wing configuration and an isolated nacelle were used as a starting point. To benefit from the potential of OWN the need of change in design of the wing arises, especially in the area in front of the installed engine. Moreover, the embedded nacelle design cannot be done separated anymore but strongly interacts with the wing and depends on the flowfield of the wing. To eliminate the separation which occurred on both sides of the nacelle a design change is required to counter the stall in these areas.

In addition to the evaluation of the design speed of flight, a Ma number variation showed that a further reduction of angle of attack and drag might be possible for high speed conditions by installing the OWN even further down in flow direction. This needs to be tested to find if there is a more favourable position for a design change in nacelle and wing shape than the candidate one found in this study.

NOMENCLATURE

Abbreviations

ACARE	Advisory Council for Aeronautics Research in Europe
BPR	Bypass Ratio
CFD	Computational Fluid Dynamics
CRC	Collaborative Research Centre
OWN	On-Wing-Nacelle
PAX	Passengers
RANS	Reynolds Averaged Navier Stokes
STOL	Short Take-off And Landing
UHBR	Ultra-High-Bypass Ratio

WB	Wing-Body
WBE	Wing-Body-Engine

Symbols

α	Angle of Attack
η	Non-dimensional longitudinal dimension
c	Chord length
C_D	Drag coefficient
C_L	Lift coefficient
c_p	Pressure coefficient
F	Thrust
Ma	Mach number
$\dot{m}$	Mass flow
x	axial position

ACKNOWLEDGMENTS

Financial support has been provided by the German Research Foundation (Deutsche Forschungsgemeinschaft – DFG) in the framework of the Collaborative Research Centre SFB 880. Computational Resources have been provided by the North-German Supercomputing Alliance (HLRN).

REFERENCES

[1] CentaurSoft, 2017, www.centaursoft.com

[2] Delfs, J, Appel, C, Bernicke, P, Blech, C, Blinstrub, J, Heykena, C, Kumar, P, Kutscher, K, Lippitz, N, Rossian, L, Savoni, L, Lummer, M "Aircraft and technology for low noise short take-off and landing", 2017, 35th AIAA Applied Aerodynamics Conference Denver, Colorado

[3] DLR "TAU-Code User Guide", Release 2014.1.0, 2014, DLR

[4] European Commission "Flightpath2050 – Europe's Vision for Aviation, Report on the High Level Group on Aviation Research", ISBN 978-92-79-19724-6, 2011, www.acare4europe.org

[5] Fujino, M, Kawamura, Y, "Wave Drag Characteristics of an Over-the-Wing Nacelle Business Jet Configuration" Journal of Aircraft, 2003, Volume 40, Number 6.

[6] Heinze, W and Weiss, T, "Main Data Sheet. A/C Type: SFB 880 Reference Aircraft REF3", 2015, Project Data Sheet

[7] Hooker, JW, Wick, A., Zeune, C, and Agelastos, A, "Over Wing Nacelle Installations for Improved Energy Efficiency" 31st AIAA Applied Aerodynamics Conference, San Diego, CA, 2013

[8] Menter, FR, "Two-equation eddy-viscosity turbulence models for engineering applications", AIAA Journal, 1994, Vol. 32, No. 8

[9] Radespiel, R, Bertsch, L, Heinze, W, "High-Lift Reasearch for Future Transport Aircraft", 2017 DLRK Munich